Arab J Sci Eng (2016) 41:4247–4262
DOI 10.1007/s13369-016-2028-3

RESEARCH ARTICLE - MECHANICAL ENGINEERING

CFD Simulations of Film Cooling Effectiveness and Heat Transfer for Annular Film Hole

Antar M. M. Abdala[1] · **Fifi N. M. Elwekeel**[2]

Received: 12 August 2015 / Accepted: 18 January 2016 / Published online: 2 February 2016

Abstract The increasing turbine entry temperature has placed demands for improvements in engine cooling, and the work described in this paper is the development of a new film cooling configuration to meet this demand. In this study, numerical simulations were performed to predict the improvement in film cooling performance with novel film hole called an annular film hole. The film cooling performance parameters such as heat transfer coefficient (h), film cooling effectiveness (η) and the net heat flux reduction (NHFR) over flat plate were investigated and compared with other configurations. Velocity profiles, pressure coefficient and turbulence kinetic energy contours were discussed. Four mass flow rates of secondary flow fluid were used to investigate the effects of film coolant velocity on the film cooling performance behavior. Results indicate that an annular film hole gives high film effectiveness, low heat transfer coefficient and higher NHFR compared to rectangular and circular film holes. The average values of laterally averaged film cooling effectiveness of the annular film hole increased to 106 and 328.5 % compared with the rectangular and circular film holes at moderate flow rate, respectively. This difference is attributable to decreasing the jet vertical velocity component in a case of the annular hole. Also the low and high heat transfer coefficient regions were described for annular hole in detail.

✉ Antar M. M. Abdala
antar451@yahoo.com

Fifi N. M. Elwekeel
fifinew2000@yahoo.com

[1] Faculty of Engineering, Matareya Branch, Helwan University, Cairo 11718, Egypt

[2] Faculty of Industrial Education, Helwan University, Cairo, Egypt

Keywords Film cooling · Adiabatic effectiveness · Heat transfer coefficient · Jet interaction phenomena

List of symbols

C_P	Pressure coefficient (–), $C_P = \frac{P-P_\infty}{0.5*\rho_\infty*u_\infty^2}$
D_h	Hydraulic hole diameter (m)
DR	Density ratio of coolant to mainstream, ρ_c/ρ_∞ (–)
h	Heat transfer coefficient (W/m^2 K)
L	Hole length (m)
M	Blowing ratio of coolant to mainstream $M = DR * U_c/U_\infty$ (–)
NHFR	Net heat flux reduction, NHFR $= 1-\frac{h}{h_o}(1-\eta*\varphi)$
P	Pressure of the fluid (Pa)
$\dot{q}$	Heat flux rate (W/m^2)
Re_{D_h}	Reynolds number based on u_∞ and D_h $Re_{D_h} = \rho u_\infty D_h/\mu$
S	Hole spacing (m)
T	Temperature (K)
Tu	Mainstream turbulence intensity (%)
u	Velocity (m/s)
X	Streamwise coordinate along model surface (m)
Y	Vertical coordinate (m)
Yplus	Non-dimensional wall distance

Greek symbols

φ	Inverse of non-dimensional metal temperature, $(T_\infty - T_c)/(T_\infty - T_w)$
α	Coolant injection angle (°)
η	Adiabatic effectiveness, $(T_\infty - T_{aw})/(T_\infty - T_c)$
θ	Non-dimensional temperature ratio, $(T_\infty - T)/(T_\infty - T_c)$
ρ	Density (kg/m^3)

Subscripts

∞ Mainstream
aw Adiabatic wall
c Coolant
o without film cooling
w Wall

1 Introduction

Modern gas turbines are designed to run at high turbine inlet temperatures well in excess of current metal temperature limits to improve thermal efficiency and power output [1]. In addition to improved temperature capability materials and TBCs, highly sophisticated cooling techniques such as augmented internal cooling and external film cooling must be used to maintain acceptable life and operational requirements under such extreme heat load conditions. Film cooling is the introduction of a secondary fluid (coolant or injected fluid) at one or more discrete locations along a surface exposed to a high-temperature environment to protect that surface not only in the immediate region of injection but also in the downstream region, and this technique will used in this paper.

Several researches and development activities proved that using cylindrical holes in film cooling had disadvantages in gas turbine applications because the jet lifts off the surface, particularly at higher momentum flux ratios (∼1 and above) leading to deterioration in the film cooling performance. Therefore, the research for new developments to optimize film cooling performance has been intensified in recent years.

The film cooling performance parameters such as heat transfer coefficient (h) and film cooling effectiveness (η) to find the net heat flux reduction over blade surface are dependent on the film cooling geometry and the coolant and mainstream flow fields. Some studies have focused only on the heat transfer coefficient enhancement, and others have presented only film effectiveness results, and others presented each of these parameters. In this paper, each of heat transfer coefficient and film cooling effectiveness will be studied.

1.1 A Review of Studies on Film Cooling Effectiveness

A large number of papers have been published on the topic of shaping the film cooling hole. Shaped holes have proven to provide the highest adiabatic effectiveness among film cooling configurations as investigated in Saumweber and Schulz [2], Goldstein et al. [3], Sen et al. [4], Thole et al. [5], Laveau and Abhari [6], and Gao and Han [7]. But the shaped holes are expensive to manufacture. Instead of using holes with shaped exits, Elwekeel et al. [8] and Abdala et al. [9,10] shown that using the upstream step will improve the film cooling performance. But step studies need to optimize the steps dimensions and to decrease the aerodynamic losses.

Sister hole is another technology investigated by Ely and Jubran [11] to increase cooling effectiveness by reducing pockets of reversed flow.

Nasir et al. [12] investigated triangular tabs that are located along upstream edge of the holes. These tabs increased cooling effectiveness, but this application showed increase in pressure drop. Certain configurations of cylindrical holes embedded in transverse trenches have been shown to perform similarly to shaped holes, and trenches would be cheaper to manufacture than shaped holes. Several studies have investigated various trench configurations such as Bunker [13], Abdala et al. [14,15], Harrison and Bogard [16], Waye and Bogard [17], Zuniga and Kapat [18].

1.2 A Review of Studies on Heat Transfer Coefficient

Heat transfer coefficients downstream of film injection are enhanced due to increased turbulence produced by mixing of the coolant jets with the mainstream boundary layer. This increased turbulence locally enhances the heat transfer coefficients [1]. Goldstein et al. [19] used a naphthalene sublimation to study the film cooling performance through a row of film holes. They showed the regions of high and low mass/heat transfer around injection holes. Ammari et al. [20] presented a summary of results for film cooling on a flat surface with a single row of holes inclined at 35° along the mainstream direction. They showed that the heat transfer coefficient ratio decreases with increasing axial distance from the injection hole. About 15-hole diameter downstream of injection, the film cooling effect disappears. The heat transfer coefficient ratio is almost equal to unity. Hay et al. [21] presented the variation of the heat transfer coefficient ratio with the blowing ratio. They showed the effect of the blowing ratio increases the heat transfer coefficient ratio. The ratio is closer to unity at lower blowing ratios, but increases to significantly high values at high blowing ratios. Ammari et al. [19] also presented the effect of density ratio on heat transfer coefficient ratio for two different coolant-to-mainstream density ratios of 1 and 1.52. It was observed that lower-density injectant provides higher heat transfer coefficient at the same blowing ratio due to higher momentum. Sen et al. [4] and Ekkad et al. [22] studied the effect of compound angle holes on heat transfer coefficients. They showed that compound angle injection provides higher heat transfer coefficients than simple angle holes. This may be due to increased lateral mixing of jets with the mainstream producing increased local turbulence and thus enhancing heat transfer coefficients. This effect increases with higher blowing ratios. Gritsch et al. [23] presented heat transfer coefficient measurements for cylinder hole with fan-

shaped hole and laidback fan-shaped hole configurations. The heat transfer coefficient ratios are highest for the cylinder hole.

With increasing blowing ratios, the heat transfer coefficient ratio increases. Heat transfer coefficients for the fan-shaped holes are much lower due to increased cross-sectional area at hole exits. This decreases the momentum of the jet and reduces penetration into the mainstream. Rhee et al. [24] conducted an experimental study to measure the local film cooling effectiveness, and the heat transfer coefficient for four different cooling hole shapes such as a straight rectangular hole, a rectangular hole with laterally expanded exit, a circular hole and a two-dimensional slot is tested. The results showed that the rectangular holes provide better performance than the cylindrical holes. For the rectangular holes with laterally expanded exit, the penetration of jet is reduced significantly, and the higher and more uniform cooling performance is obtained even at relatively high blowing rates. The reason is that the rectangular hole with expanded exit reduces momentum of coolant and promotes the lateral spreading like a two-dimensional slot.

1.3 Two-Equation Turbulence Models

Two-equation turbulence models are very widely used, as they offer a good compromise between numerical effort and computational accuracy. Two-equation models are much more sophisticated than the zero-equation models. Both the velocity and length scale are solved using separate transport equations (hence the term 'two-equation' model).

The k-ε and k-ω two-equation models use the gradient diffusion hypothesis to relate the Reynolds stresses to the mean velocity gradients and the turbulent viscosity. The turbulent viscosity is modeled as the product of a turbulent velocity and turbulent length scale.

In two-equation models, the turbulence velocity scale is computed from the turbulent kinetic energy, which is provided from the solution of its transport equation. The turbulent length scale is estimated from two properties of the turbulence field, usually the turbulent kinetic energy and its dissipation rate. The dissipation rate of the turbulent kinetic energy is provided from the solution of its transport equation.

1.3.1 The k-Epsilon Model in ANSYS CFX

k is the turbulence kinetic energy and is defined as the variance of the fluctuations in velocity. It has dimensions of ($L^2 T^{-2}$), for example m^2/s^2. ε is the turbulence eddy dissipation (the rate at which the velocity fluctuations dissipate) and has dimensions of per unit time (L^2T^{-3}), for example m^2/s^3.

The k-ε model introduces two new variables into the system of equations. The continuity equation is then:

$$\frac{\partial \rho}{\partial t} + \frac{\partial}{\partial x_i}(\rho U_i) = 0, \tag{1}$$

and the momentum equation becomes:

$$\frac{\partial}{\partial t}(\rho U_i) + \frac{\partial}{\partial x_j}(\rho U_i U_j) = -\frac{\partial p'}{\partial x_i} + \frac{\partial}{\partial x_j}\left[\mu_{\text{eff}}\left(\frac{\partial U_i}{\partial x_j} + \frac{\partial U_j}{\partial x_i}\right)\right] + S_M \tag{2}$$

where S_M is the sum of body forces, μ_{eff} is the effective viscosity accounting for turbulence, and p' is the modified pressure defined as follows:

$$p' = p + \frac{2}{3}\rho k + \frac{2}{3}\mu_{\text{eff}}\frac{\partial U_k}{\partial x_k} \tag{3}$$

The k-ε model, like the zero-equation model, is based on the eddy viscosity concept, so that:

$$\mu_{\text{eff}} = \mu + \mu_t \tag{4}$$

where μ_t is the turbulence viscosity. The k-ε model assumes that the turbulence viscosity is linked to the turbulence kinetic energy and dissipation via the relation:

$$\mu_t = C_\mu \rho \frac{k^2}{\varepsilon} \quad C_\mu = 0.09. \tag{5}$$

The values of k and ε come directly from the differential transport equations for the turbulence kinetic energy and turbulence dissipation rate:

$$\frac{\partial(\rho k)}{\partial t} + \frac{\partial}{\partial x_j}(\rho k \mathbf{U}_j) = \frac{\partial}{\partial x_j}\left[\left(\mu + \frac{\mu_t}{\sigma_k}\right)\frac{\partial k}{\partial x_j}\right] + P_k - \rho\varepsilon + P_{kb} \tag{6}$$

$$\frac{\partial(\rho \varepsilon)}{\partial t} + \frac{\partial}{\partial x_j}(\rho \varepsilon \mathbf{U}_j) = \frac{\partial}{\partial x_j}\left[\left(\mu + \frac{\mu_t}{\sigma_\varepsilon}\right)\frac{\partial \varepsilon}{\partial x_j}\right] + \frac{\varepsilon}{k}\left(C_{\varepsilon 1} P_k - C_{\varepsilon 2}\rho\varepsilon + C_{\varepsilon 1} P_{\varepsilon b}\right) \tag{7}$$

The model constants used in the above equations have following default values:

$$C_{\varepsilon 1} = 1.44, \quad C_{\varepsilon 2} = 1.92, \quad \sigma_k = 1.0, \quad \sigma_\varepsilon = 1.3$$

P_{kb} and $P_{\varepsilon b}$ represent the influence of the buoyancy forces. P_k is the turbulence production due to viscous forces.

1.3.2 The k-Omega Model in ANSYS CFX

This model does not involve the complex nonlinear damping functions required for the k-ε model and is therefore more accurate and more robust.

The k-ω models assume that the turbulence viscosity is linked to the turbulence kinetic energy and turbulent frequency via the relation:

$$\mu_t = \rho \frac{k}{\omega} \tag{8}$$

The starting point of the present formulation is the k-ω model developed by Wilcox [25]. It solves two transport equations: one for the turbulent kinetic energy, k, and one for the turbulent frequency, ω. The stress tensor is computed from the eddy viscosity concept.

k-equation:

$$\frac{\partial(\rho k)}{\partial t} + \frac{\partial}{\partial x_j}(\rho k \mathbf{U}_j) = \frac{\partial}{\partial x_j}\left[\left(\mu + \frac{\mu_t}{\sigma_k}\right)\frac{\partial k}{\partial x_j}\right] + P_k - \beta' \rho k \omega + P_{kb} \tag{9}$$

ω-equation:

$$\frac{\partial(\rho \omega)}{\partial t} + \frac{\partial}{\partial x_j}(\rho \omega \mathbf{U}_j) = \frac{\partial}{\partial x_j}\left[\left(\mu + \frac{\mu_t}{\sigma_\omega}\right)\frac{\partial \omega}{\partial x_j}\right] + \alpha \frac{\omega}{k} P_k - \beta \rho \omega^2 + P_{\omega b} \tag{10}$$

In addition to the independent variables, the density, ρ, and the velocity vector, $\mathbf{U}$, are treated as known quantities from the Navier–Stokes method. P_k is the production rate of turbulence, which is calculated as in the k-ε model. The model constants are given by:

$$\beta' = 0.09 \tag{11}$$

$$\alpha = 5/9 \tag{12}$$

$$\beta = 0.075 \tag{13}$$

$$\sigma_k = 2 \tag{14}$$

$$\sigma_\omega = 2 \tag{15}$$

The unknown Reynolds stress tensor, $\rho\overline{u_i u_j}$, is calculated from:

$$R_{ij} = -\rho\overline{u_i u_j} = \mu_T\left(\frac{\partial U_i}{\partial x_j} + \frac{\partial U_j}{\partial x_i}\right) - \frac{2}{3}\mu_T \frac{\partial U_k}{\partial x_k}\delta_{ij} - \frac{2}{3}\rho k \delta_{ij} \tag{16}$$

The above review revealed that the development of film cooling has aimed at producing high film effectiveness and low heat transfer coefficient, with uniform protection of the surface, using the minimum amount of coolant air to minimize the penalty of using film cooling. The film cooling performance is highly dependent on the configuration, so investigating variations in depth, width and shape is important to maximize the effectiveness. The time now is to know the behavior of the secondary flow fluid emanating from another film hole than circular or rectangular film holes.

In this paper, a novel development used is called annular film cooling hole to improve the film cooling performance. Film cooling effectiveness, heat transfer coefficient and net heat flux ratio over flat plate surface will be investigated by using ANSYS CFX. The influence of the mass flow rates of secondary flow fluid on film cooling performance will be investigated. Velocity profiles, pressure coefficient and turbulence kinetic energy contours will be discussed. The low and high heat transfer coefficient regions were described for annular hole in detail.

2 Computation Setup

An outline of the geometry for the annular film cooling hole is shown in Fig. 1. The hydraulic diameter of annular film hole is 10 mm with inner and outer diameters 10 and 20 mm, respectively. This study represents the initial screening calculations to determine the feasibility of this idea by using CFD simulations. But in a real situation, the central pin needs a joint with other components (struts or something else). For a film hole technically manufacturability, drilling or EDM cannot be applied. It may be by direct casting or by additive

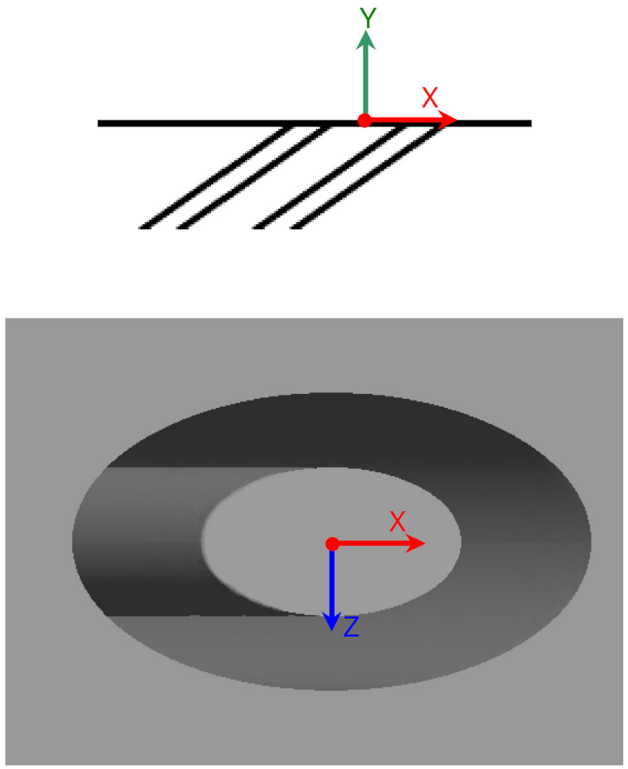

Fig. 1 Annular film hole under test

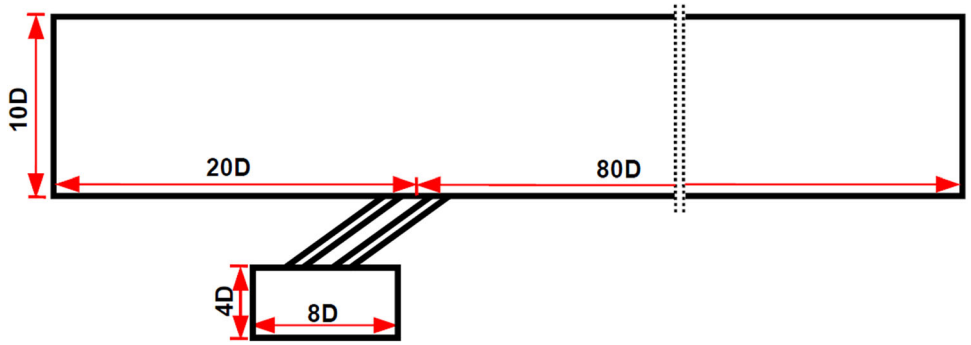

Fig. 2 Dimensions of computational domain

Table 1 Simulation parameter conditions

Configuration dimensions		Mainstream conditions	
D_h	10 (mm)	Tu	0.5 %
α	35°	u_∞	15 (m/s)
L/D	6.97	T	293 (K)
S/D	3	DR	0.93 (η)
Re_{D_h}	9869	DR	1 (h)
		M	0.5, 1, 1.5, 2

manufacturing. These are practical issues which would have to be weighed against the expected performance gain.

The coordinate origin $X/D = 0$ for annular film hole was defined as the center of the hole. Dimensions of computational domain are illustrated in Fig. 2.

In this study, a grid sensitivity study was carried out to determine the appropriate grid for Rhee et al. [24]. Five grids for heat transfer coefficient simulation—the baseline grid with 1.9 million cells and a finer grid with 2.9, 4.3, 5.6 and 13 million cells (adaptation)—were used. For all finer grids, the additional cells were all concentrated about the film cooling hole and the hot gas/coolant jet interaction regions, where the flow physics is most complicated. From this grid sensitivity study, an adaptation with 4.3 million cells was found to give essentially the same result for heat transfer coefficient. The final mesh sizes for annular film hole were 8.6 million cells for heat transfer coefficient and 11.7 million cells for film cooling effectiveness. Simulation conditions are presented in Table 1. The results obtained in the current study were generated using ANSYS CFX code K-ω turbulence model for (h) simulations and K-ε for (η). A very fine region of cells was created on the walls to approximate Y^+ values less than unity as shown in Fig. 3. The convergence criterion was set to RMS residuals of 1×10^{-5}. Computations were performed on a high-performance parallel computer cluster equipped with 20 computer nodes with Intel CPUs and 200 cores.

All flow inlets were defined as velocity inlets, while the outlet was defined as a pressure outlet. Due to symmetry, the model was cut along its half-plane and a symmetry boundary

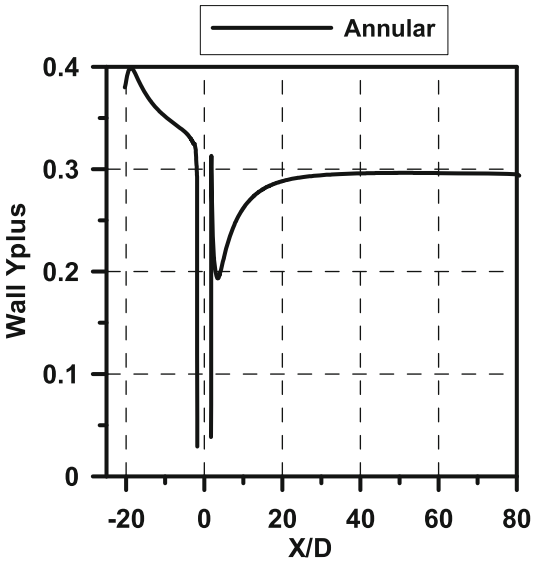

Fig. 3 Yplus distribution of the first mesh near the wall

condition was applied. The plate wall was assigned heated wall ($q = 2000\,\mathrm{W/m^2}$) for (h) and was assigned adiabatic wall with no-slip conditions for (η).

The hole and the plenum walls were assigned adiabatic walls with no-slip conditions.

The top of the tunnel and the remaining plane were assigned walls with free slip conditions. Air was taken as a working fluid with Prandtl number value equal to 0.705.

The density was modeled as a perfect gas. The plenum inlet velocity was varied to simulate different mass flow rates equivalent to the blowing ratios $M = 0.5$, 1, 1.5 and 2.

3 Heat Transfer Coefficient and Film Cooling Effectiveness Equations

There are a lot of published papers that used heat transfer and film cooling effectiveness equations, and in this paper, the equations of Rhee et al. [24] will be used.

In general, heat transfer to a film-cooled surface is expressed as follows:

$$\dot{q} = h(T_w - T_{aw}) \tag{17}$$

The film cooling effectiveness is used as a dimensionless form of the adiabatic wall temperature and is defined as in Eq. (18) for low-speed and constant-property flows.

$$\eta = (T_{aw} - T_\infty)/(T_c - T_\infty) \tag{18}$$

The heat transfer coefficient on a surface obtained from Eq. (19) when T_{aw} is set to be equal to T_∞ is

$$h = \frac{\dot{q}_w}{(T_w - T_{aw})} = \frac{\dot{q}_w}{(T_w - T_\infty)} \tag{19}$$

The net heat flux reduction (NHFR) is used to quantify the reduction in heat transfer to the blade with film cooling as compared to without film cooling.

NHFR is defined as:

$$\text{NHFR} = 1 - \frac{\dot{q}_w}{\dot{q}_o} = 1 - \frac{h}{h_o}(1 - \eta * \varphi) \tag{20}$$

As defined in Eq. (20), NHFR combines the effects of two parameters: heat transfer coefficient and film cooling effectiveness. In the present study, φ is set to be a typical value of 1.5 for gas turbine blade applications.

4 Results

In the present work, the computational domain was validated by experimental work. Contours and thermal profiles for film cooling effectiveness and heat transfer coefficients of annular film hole were drawn and compared with the other configurations.

5 Rectangular and Circular Holes Benchmark

A comprehensive sensitivity analysis was performed against the experimental works [17,24] for lateral film heat transfer coefficient and laterally adiabatic film effectiveness as a function of dimensionless downstream distance as shown in Figs. 4, 5 and 6. The trends of (h) data follow that of Rhee et al. [24]. k-ω turbulence model results offer more realistic data and best agreement than k-ε turbulence model. This is because k-ε model calculates the turbulence kinetic energy (k), the turbulence viscosity (μ_t) and the strain rate with higher levels, leading to increasing turbulence levels of heat transfer coefficient.

The trends of (η) data follow that of Rhee et al. [24] and Waye and Bogard [17]. k-ε turbulence model gives better agreement with the experiments than k-ω turbulence model. This refers to increasing the jet penetration in cross-flow by using k-ω model, leading to increasing the backflow region and drop in film cooling effectiveness calculations.

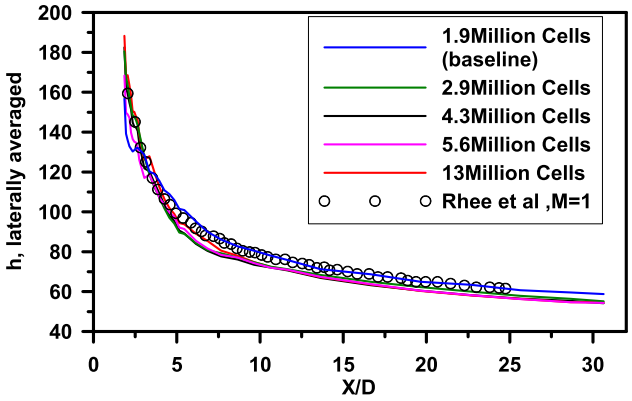

Fig. 4 Grid-independent study and validation of rectangular hole with experiment [24] for k-ω turbulence model at $M = 1$ (heat transfer coefficient)

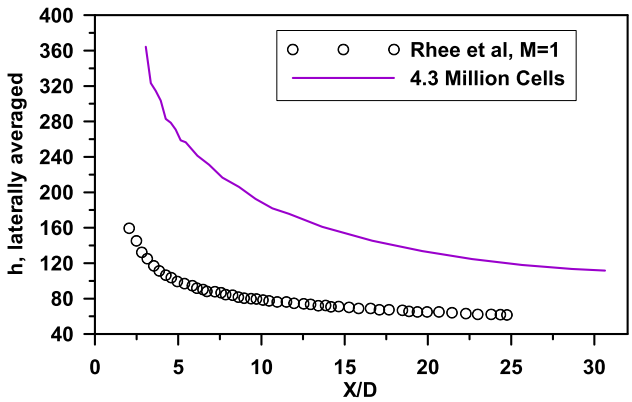

Fig. 5 Validation of rectangular hole with experiment [24] for k-ε turbulence model at $M = 1$ (heat transfer coefficient)

5.1 Laterally Adiabatic Film Effectiveness

Comparisons for annular hole with experimental work Rhee et al. [24] are shown in Figs. 7 and 8. Rhee et al. [24] proved that rectangular cross section outperformed the circular cross section at all blowing ratios, so most of the comparisons will be executed using rectangular film hole which has a higher film cooling performance levels.

At a low blowing ratio ($M = 0.5$), the film cooling effectiveness of annular film hole outperforms the rectangular and circular film holes with average values 51.2 and 130.4 %, respectively, because the annular film hole helps in decreasing the jet velocity. At a moderate blowing ratio ($M = 1$), the film cooling effectiveness outperforms the rectangular and circular film holes with average values 106 and 328.5 %, respectively. It is clear that the jet separation is lower for annular hole than for rectangular and circular holes due to decreasing jet vertical velocity component in case of annular

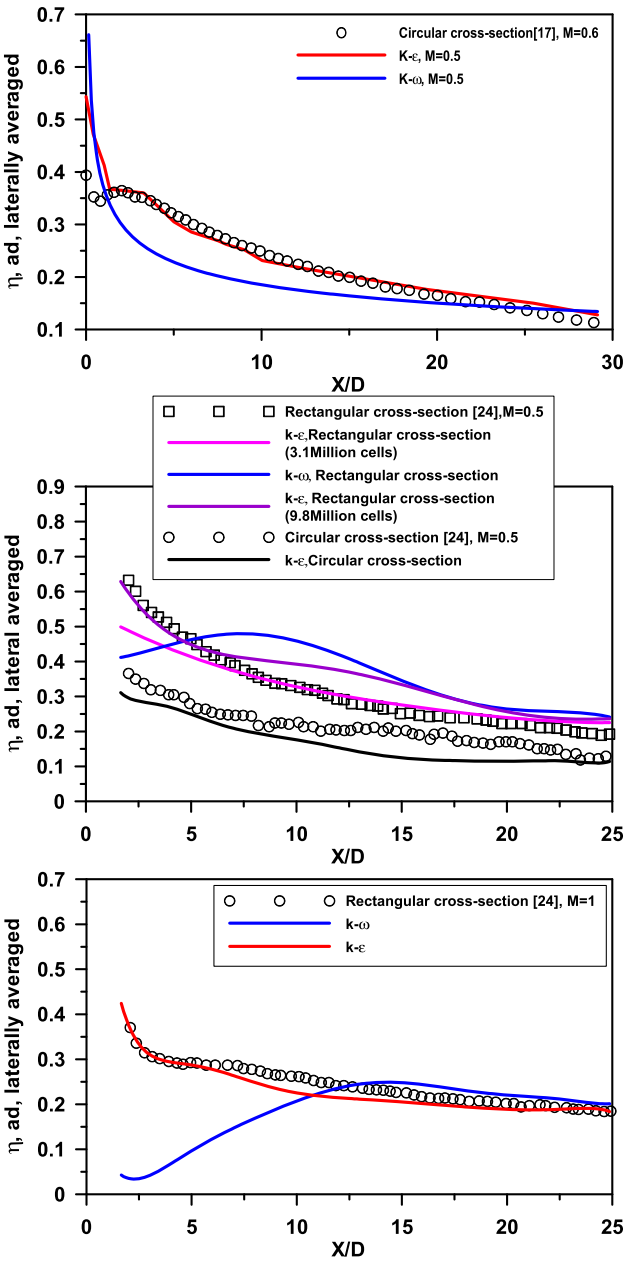

Fig. 6 Validation of rectangular and circular film holes with experiments (film cooling effectiveness)

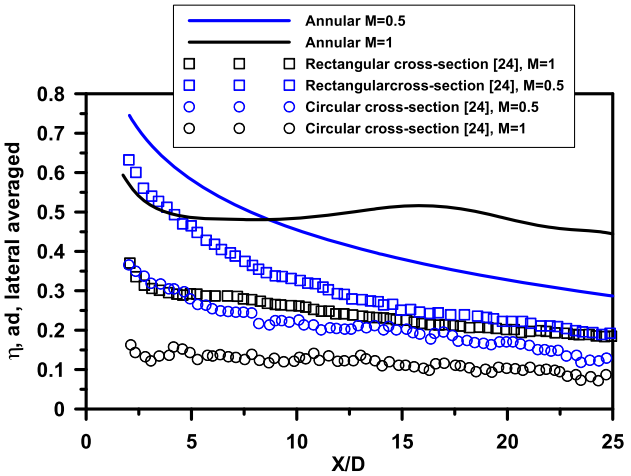

Fig. 7 Laterally averaged adiabatic film effectiveness for annular hole case and experiment [24]. At $M = 0.5$ and 1

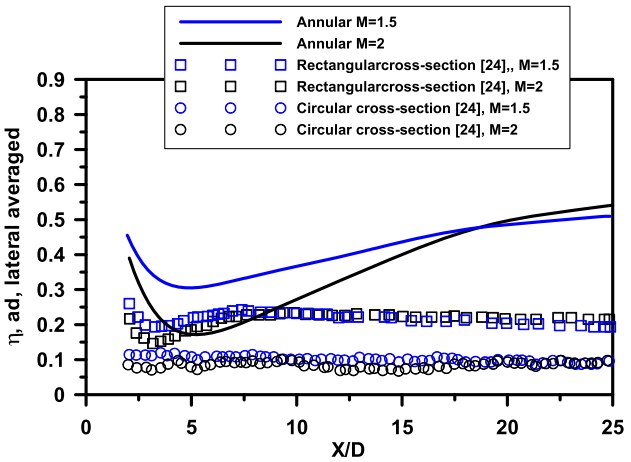

Fig. 8 Laterally averaged adiabatic film effectiveness for annular hole case and experiment [24]. At $M = 1.5$ and 2

film hole. At high blowing ratios ($M = 1.5$ and $M = 2$), the jet separation and reattachment for annular film hole occurs as for the rectangular and circular film holes since the values decreased adjacent to the holes and then increased again. But still the values of film cooling effectiveness for annular case is higher than rectangular and circular cases with 88, 289.5 and 63, 289.7 % for $M = 1.5$ and $M = 2$, respectively.

Figure 9 shows film cooling effectiveness distributions for annular film hole over the flat plate at different blowing ratios. It is clear that film cooling effectiveness distributions in lateral direction at $M = 0.5$ and $X/D \leq 10$ is wider than the other blowing ratios. The interactions and mixing between the mainstream and jet at $X/D > 10$ and $M = 0.5$ are strong, leading to a decrease in film cooling effectiveness distributions in centerline and lateral directions. It is clear that the centerline effectiveness distributions for $M = 1$ are longer than other blowing ratios until $X/D \leq 20$, while at blowing ratios $M = 1.5$ and $M = 2$, the jet separates and reattaches shortly on the surface (at $X/D = 4{:}5$) and then film cooling effectiveness distributions increase in centerline and lateral directions.

Figure 10 shows thermal profiles for the annular film hole for $M = 0.5$ and $M = 1$ at $X/D = 5$ and $X/D = 10$. In all profiles, thermal contours are circular, with a kidney-shaped contour in the center. Simulations showed that the coolant jet for annular film hole has attached on the surface at $M = 0.5$, but at $M = 1$ the simulation showed that core jet little attached on the surface. Also simulations predict lower

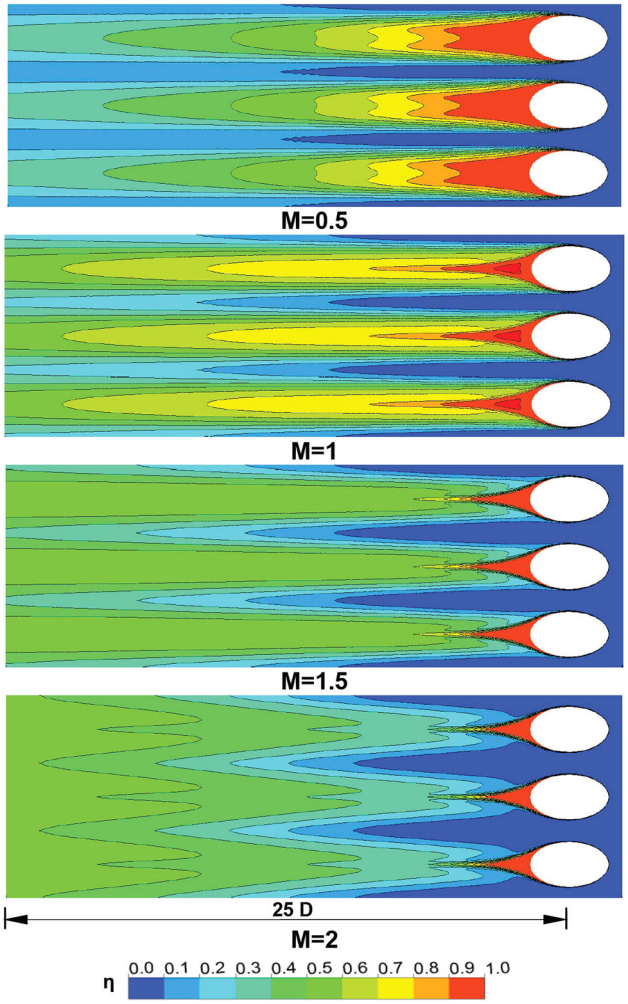

Fig. 9 Film cooling effectiveness contours for annular film hole

temperatures (higher θ) at the center of the jet profile at the downstream.

Figure 11 presents centerline thermal profiles for annular film hole. It is clear that at M = 0.5 and 1, the jet still attaches on the surface and there is no lift off due to decreased jet vertical momentum. At high blowing ratios ($M = 1.5$ and 2), the jet starts to lift off at $X/D = 4{:}5$ and then reattaches on the surface.

The study of Rhee et al. [24] did not present centerline thermal profiles above the flat plate, but these are easy to examine with CFD. Figure 12 shows comparison between the centerline thermal profiles for annular and simulated rectangular film holes at $M = 1$. It is clear that the jet still hugs the surface for annular configuration compared to the rectangular configuration due to decreasing vertical velocity component of the jet in the case of annular configuration.

A new correlation is proposed to predict the film cooling effectiveness for annular film hole at different blowing ratios as shown in Fig. 13. The film effectiveness performance for varying blowing ratios can be scaled using the parameter X/MS_e, where S_e is the 'equivalent slot length' with $S_e = A_{\text{hole}}/\text{S}$, where A_{hole} is the cross-sectional area of the coolant hole and S is the pitch between holes [26]. The new correlations were divided into ranges, for low blowing ratios $M \leq 1$ where the jet tries to keep without separation and for high blowing ratios $M > 1$ where the jet detached over the surface.

For $M \leq 1$

$$\eta, \text{ ad, laterally averaged } = -0.005853583037^*(X/MS_e) + 0.6159532281$$

For $M > 1$

$$\eta, \text{ ad, laterally averaged} = a_0 + a_1{}^*(X/MS_e) + a_2{}^*(X/MS_e)^2 + a_3{}^*(X/MS_e)^3 + a_4{}^*(X/MS_e)^4 + a_5{}^*(X/MS_e)^5 + a_6{}^*(X/MS_e)^6$$

Coefficients:

$a_0 = 0.8112517171$

$a_1 = -0.3834903134$

$a_2 = 0.09198393985$

$a_3 = -0.01002763334$

$a_4 = 0.0005756844485$

$a_5 = -1.694124301\text{E}{-}005$

$a_6 = 2.014145233\text{E}{-}007$

5.2 Near-Field Flow Phenomena

In the absence of a cross-flow, the jet behaves as a simple jet, the fluid decelerating as it moves away from the jet exit. In the absence of a jet, the cross-flow would behave as a laminar flow over a flat plate. When both are present, the jet acts as an obstacle in the path of the cross-flow. This is particularly true close to the wall. The near field and the trajectory of the jet can be explained as a result of the competing inertia of the jet and the cross-flow.

Figure 14 is a schematic of the near field of the jet exit. On the symmetry plane, the boundary can be represented by two streamlines, one beginning at the leading edge of the jet exit and the other beginning at the trailing edge. The jet acts like an obstacle in the path of the cross-flow fluid, and a region of high pressure is set up upstream of the jet as shown. Sample contours of the pressure coefficients ($C_P = \frac{P-P_\infty}{0.5^*\rho_\infty{}^*u_\infty^2}$) on the symmetry plane are shown in Fig. 14, where P_∞ is the free stream pressure at the cross-flow inlet. Note the high pressure upstream of the jet beginning close to jet exit. For annular film hole, the value of the high-pressure region is lower than for rectangular film hole.

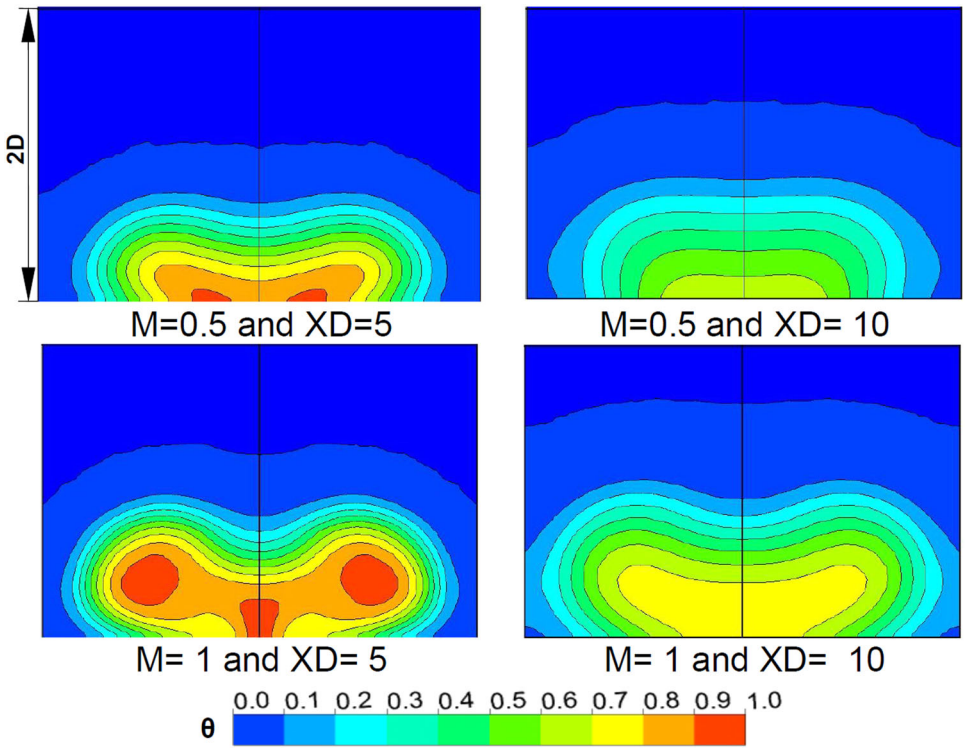

Fig. 10 Non-dimensional temperature ratio (θ) at different locations and blowing ratios

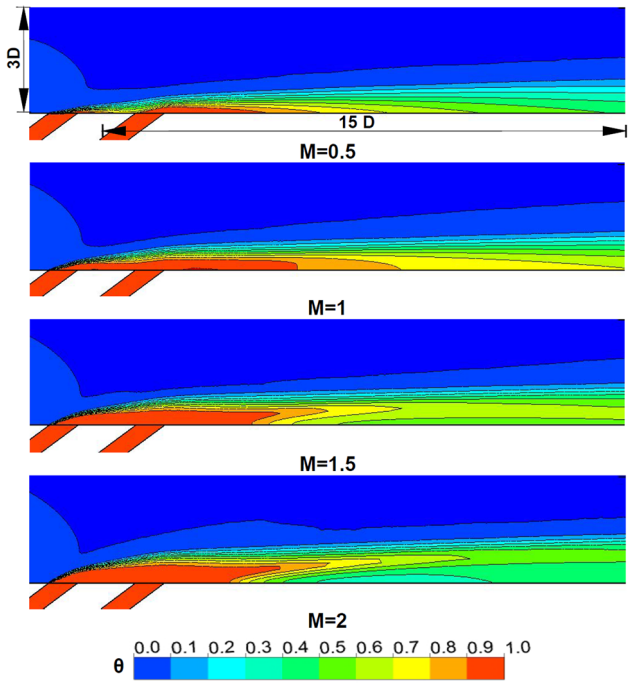

Fig. 11 Centerline thermal profiles for annular film hole at different blowing ratios

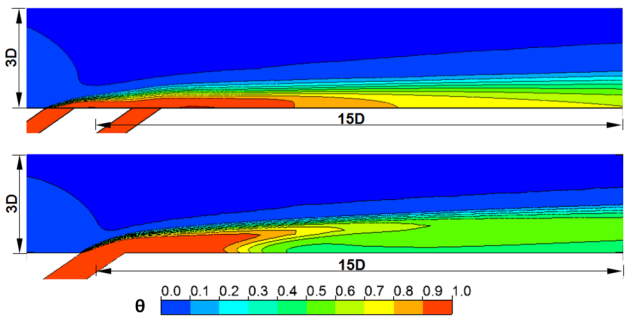

Fig. 12 Comparison between the centerline thermal profiles for annular (*top*) and simulated rectangular (*bottom*) film holes at $M = 1$

Pressure coefficient profiles correspond to vertical locations $y = 0.05D, 0.2D$ and $0.5D$ shown in Fig. 15. The first of the profiles is within the cross-flow boundary layer (where the cross-flow velocity is lower than u_∞). At the cross-flow boundary, the pressure is the free stream pressure. An increase in pressure is observed moving toward the jet, and a pressure peak is seen just upstream of the jet exit. So there are two pressure peaks for annular hole and one peak for rectangular hole. The pressure minima once past the jet exit and the profiles show steep gradients near the jet edges. Downstream of the jet exit, there is a region of pressure recovery. It is clear that the annular film hole gave high pressure coefficient values than rectangular hole. This refers to the momentum of the cross-flow fluid closer to the jet exit for rectangular hole increases. As a result, the high pressure values are increased also. It is clear that all the results showed that the peak of pressure coefficient values decreased in vertical directions (at $0.2D$ and $0.5D$).

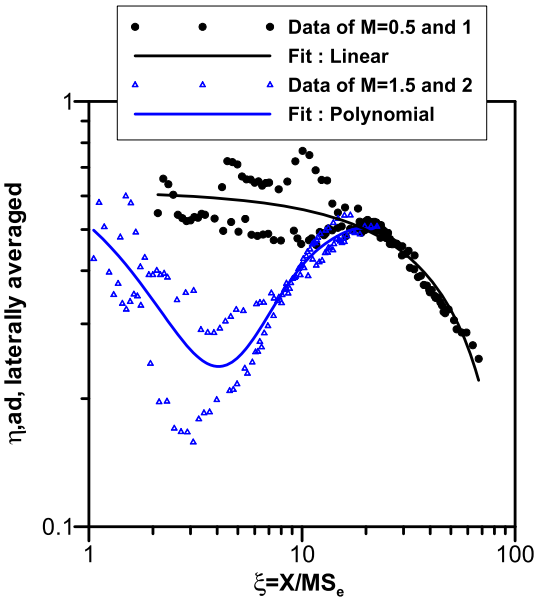

Fig. 13 Distributions of laterally averaged adiabatic film effectiveness at different blowing ratios as a function of X/MS_e

Contours of the turbulence kinetic energy k/u_∞^2 on the symmetry plane are shown in Fig. 16. There are regions of turbulence levels that can be distinguished:

1. The corner between the plenum and the downstream film hole wall, where the flow undergoes sharp 145° turn as shown for two configurations. The values of k/u_∞^2 levels for rectangular and annular configurations are about 5 % and less than 1 %, respectively.
2. A shear layer between the separated region and the 'jetting' region inside the film hole. This shear layer carries high levels of turbulence into the cross-flow region. It is clear that the annular configuration does not have this region.
3. At the trailing and leading edges of the hole exit cross section. It is cleared that the rectangular configuration has turbulence levels at trailing edge higher than the annular configurations, while at leading edge, the rectangular configuration does not have turbulence levels.
4. Immediately behind the downstream edge in which k/u_∞^2 levels are less than 1.5 % for each of the configurations.
5. The interaction between the jet and the cross-flow fluids. It is clear that the annular configuration has turbulence levels less than 1.5 %, while the rectangular configuration does not have these levels.

Figure 17 shows the variation of the horizontal and vertical components of mean velocity (u, v) along the center streamline. As the jet evolves and bends, the jet fluid accelerates in the direction of the cross-flow fluid, indicated by the increase in (u). In the far field, one would expect the jet fluid to travel in the direction of the cross-flow and, hence, the asymptotic values of the curves would be u_∞ for (u) and zero for (v). It is clear that the velocity components for annular film hole are lower than for the rectangular film hole.

Figure 18 shows the comparison between the jet trajectories obtained for annular and rectangular film holes at $M = 0.5$. The trajectories show that the fluid in the pipe exits the jet exit and interacts with the cross-flow fluid as it moves away from the jet exit and begins to bend in the direction of the cross-flow. Close to the jet exit, the trajectories are almost vertical. The jet in case of rectangular film hole penetrates deeper than the jet in case of annular film hole as expected. This difference is attributable to decreasing the jet vertical velocity component in case of annular hole.

5.3 Heat Transfer Coefficient

In all calculations of heat transfer coefficient of an annular film hole, the upstream heating length is used to approach

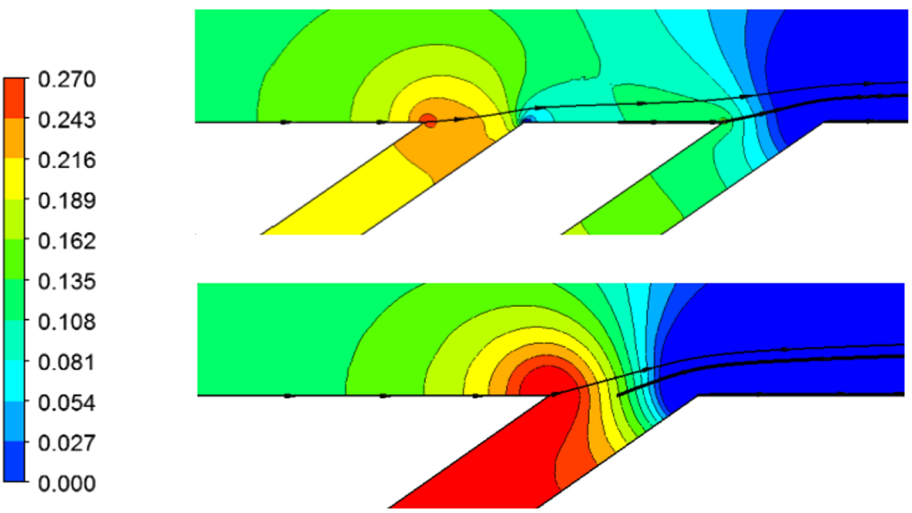

Fig. 14 Pressure coefficient contours in the jet symmetry plane for annular case (*top*) and simulated rectangular case (*bottom*) at $M = 0.5$

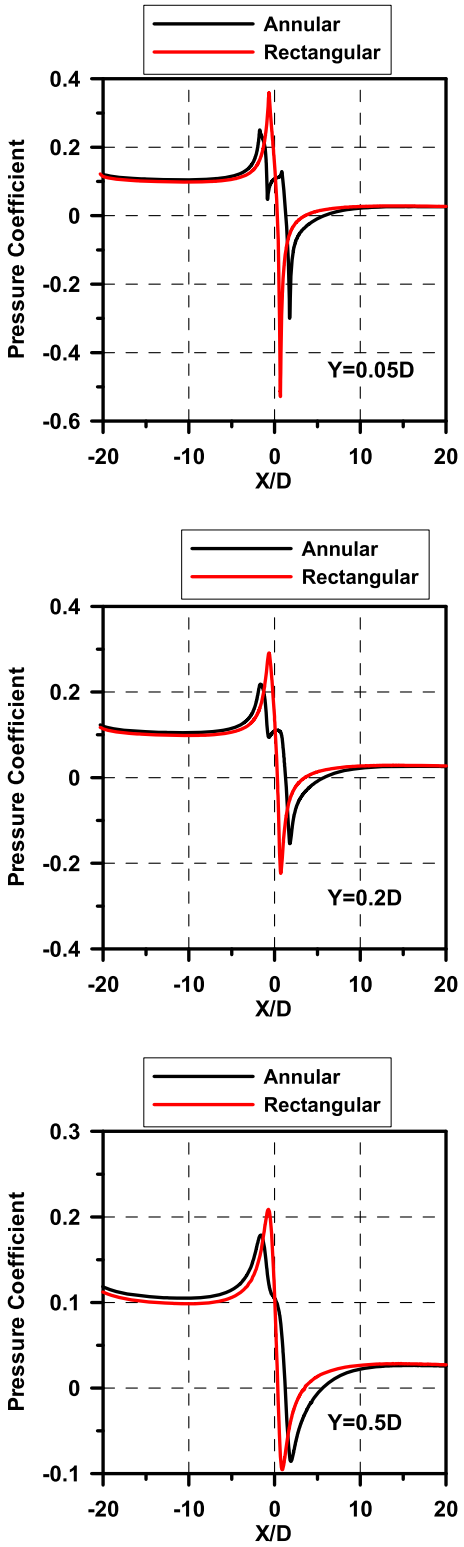

Fig. 15 Pressure coefficient for annular and rectangular cases at $M = 0.5$ at locations $Y = 0.05D$, $0.2D$ and $0.5D$

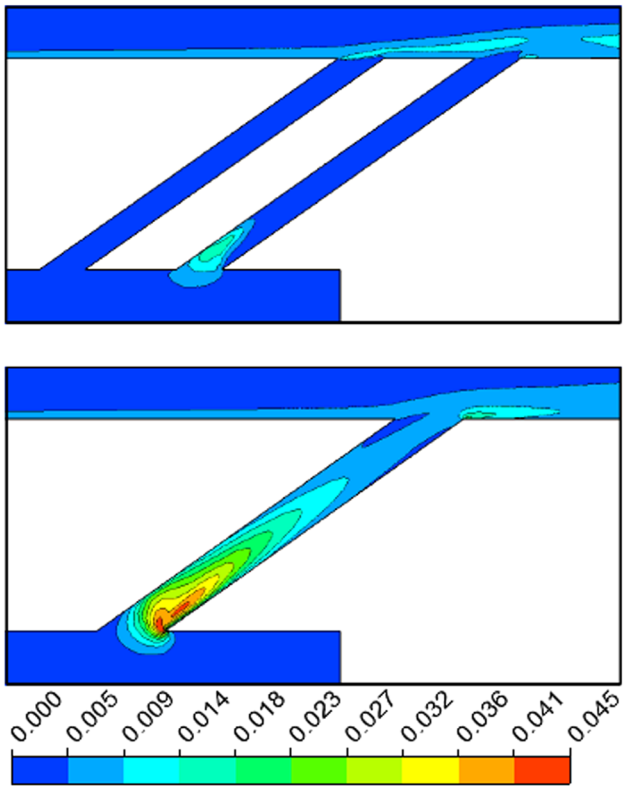

Fig. 16 Turbulence kinetic energy k/u_∞^2 on the symmetry plane for annular case (*top*) and simulated rectangular case (*bottom*) at $M = 0.5$

from the realistic airfoils. Figure 19 shows laterally averaged heat transfer coefficients for annular film hole at different blowing ratios. The heat transfer coefficient values decrease with increasing axial distance from the injection hole. The effect of the blowing ratio increases the heat transfer coefficient values. But at $M = 0.5$, there is a clear drop in heat transfer coefficient at $X/D = 5.4$ and this refers to increased temperature in this region due to fluids interaction forming vortex underneath the jet, and this vortex tries to stay in place as shown in Fig. 20. And due to the mixing between the fluids with a heated surface, all these factors try to heat this region. At $X/D > 5.4$, the heat transfer coefficient starts to increase due to interactions between the mainstream and the secondary flow, and the heat transfer coefficient average values remains mainly constant until $X/D = 25$. At $M \geq 1$ and $X/D \geq 7$, the heat transfer coefficient increases due to increased mainstream jet interaction. This refers to high blowing ratios, and the secondary flow lifts off from the wall. Due to the blockage of the mainstream by the secondary flow liftoff, the mainstream penetrates underneath the secondary flow by induced pressure deficit and sweeps toward the wall under the injected flow. At $X/D \geq 20$, the effect of film cooling disappears and heat transfer coefficient starts to decrease.

Figure 21 shows the laterally averaged heat transfer coefficients in two cases of upstream and non-upstream starting length without coolant injection. It is clear that there is a good agreement for the simulation of heat transfer coefficient in case of non-upstream heating with Rhee et al. [24].

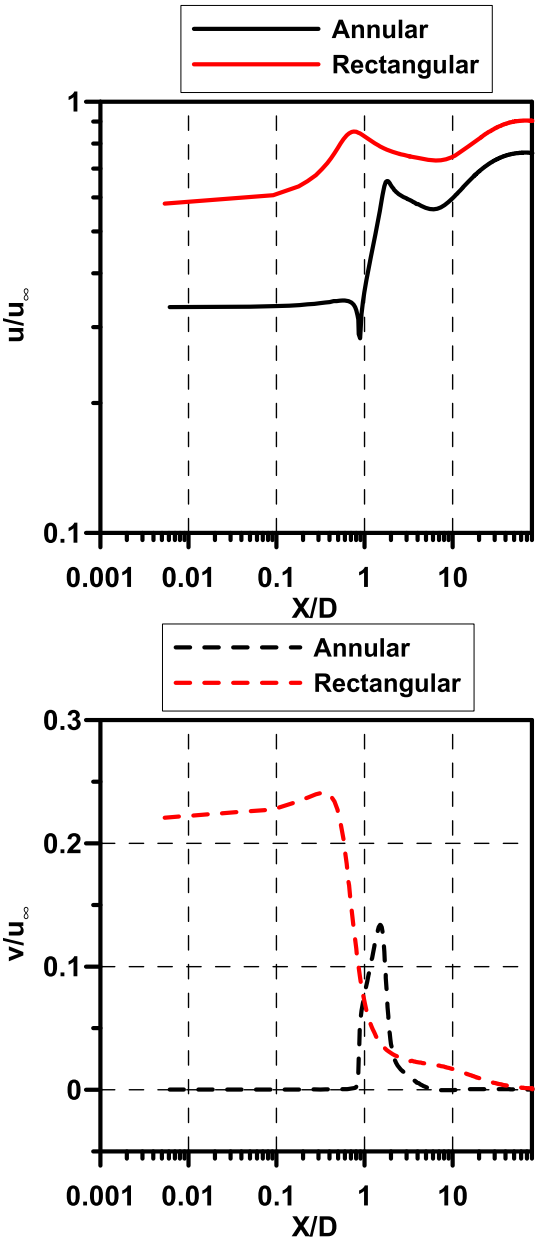

Fig. 17 Variations of velocities along the center streamline, plotted as a function of distance from the jet exit

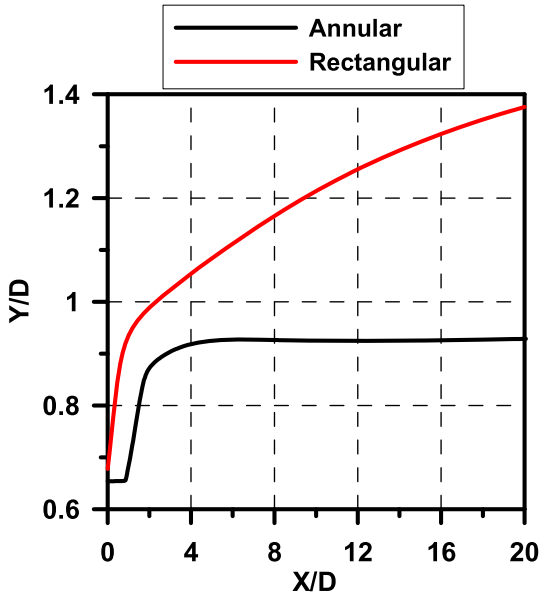

Fig. 18 Center streamline jet trajectory emanating from annular and rectangular film holes at $M = 0.5$

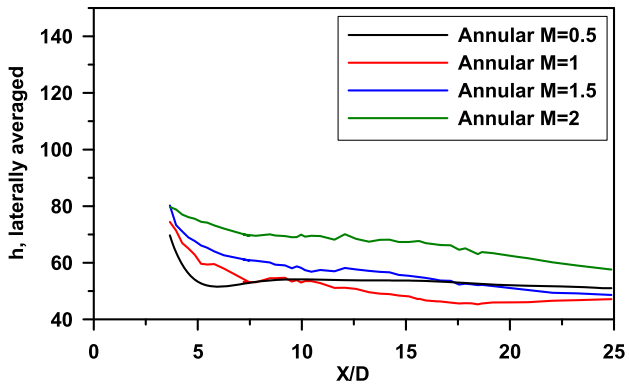

Fig. 19 Variation of laterally averaged the heat transfer coefficient with the blowing ratio for annular hole

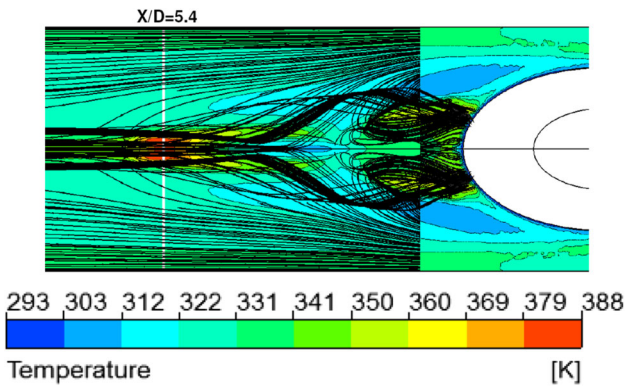

Fig. 20 Temperature contour for annular hole with streamlines at $M = 0.5$

As expected, an unheated starting length resulted in much higher heat transfer coefficient initially because of the development of a new thermal boundary layer as shown in Fig. 22 at $X/D = -5$ and 2. In Fig. 22 at $X/D = -5$, the wall temperature and the mainstream temperature are the same for case of non-heating starting length, so the difference between the temperatures is zero; therefore, the heat transfer coefficient is infinity at leading edge of flat plate (i.e., $h = \dot{q}/0 = \infty$).

Figure 23 shows area-averaged NHFR for various hole configurations. The data used in area averaging are in the region of $2.5 \leq X/D \leq 8.5$. It is clear from Fig. 23 that the values of NHFR decrease with increasing blowing rates. The annular film hole shows higher NHFR values at all blowing ratios than the other hole configurations. This increase in

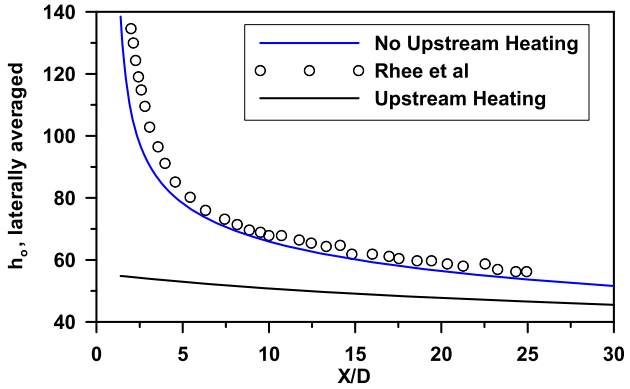

Fig. 21 Heat transfer coefficient with no film cooling hole

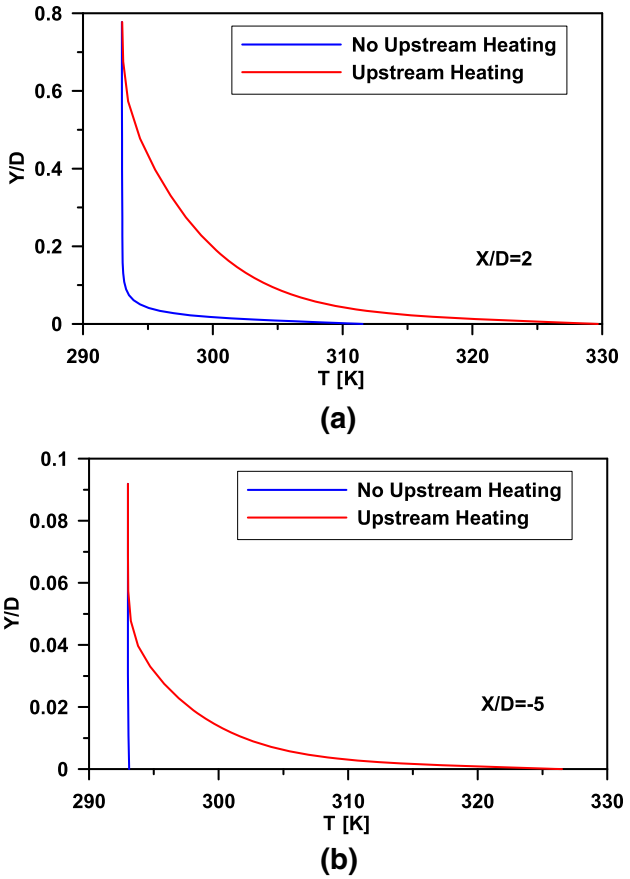

Fig. 22 Thermal boundary layer with and without upstream heating at **a** $X/D = 2$ and **b** $X/D = -5$

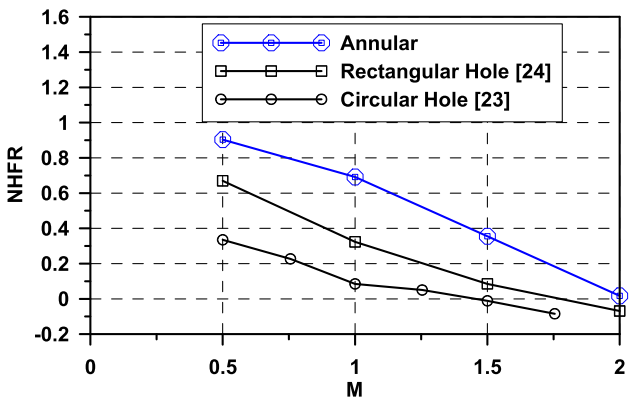

Fig. 23 Area-averaged NHFR for various hole configurations versus blowing ratios

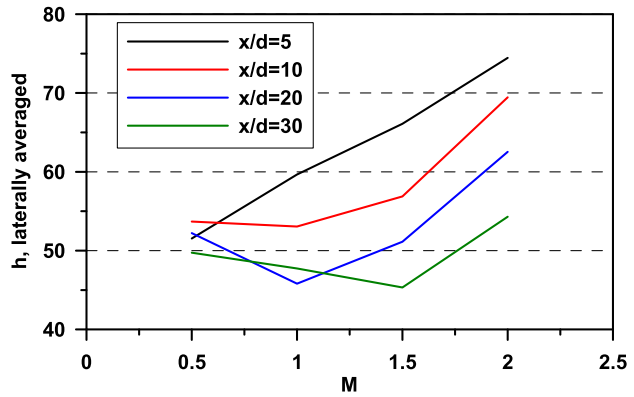

Fig. 24 Variation of laterally averaged heat transfer coefficient with the blowing ratio for annular hole at different locations

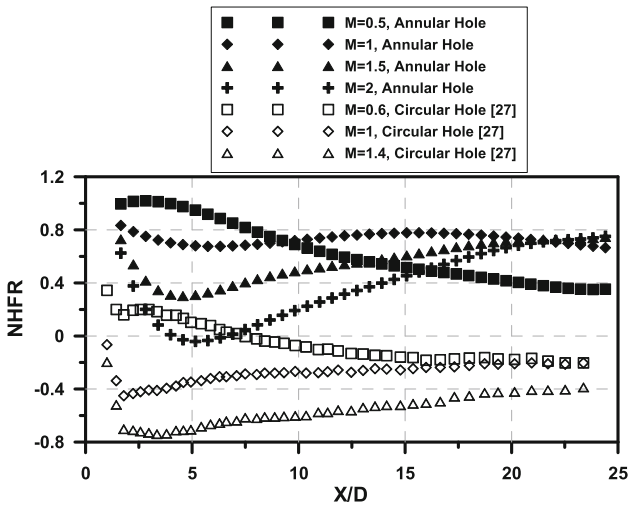

Fig. 25 Comparison of NHFR for annular and circular film holes with streamwise direction

NHFR is because the annular film hole decreases the vertical velocity component of the jet, leading to increasing film cooling effectiveness and decreasing heat transfer to the surface.

Figure 24 shows the effect of the blowing ratios on the laterally averaged heat transfer coefficient at $X/D = 5$, 10, 20 and 30. For all results, the average values increase as the blowing ratios increase. It is clear that the average values are closer at lower blowing ratio but increase to significant high values at higher blowing ratios. It is clear that at $M = 1$ and $X/D = 20$, the average values are lower than the values at $X/D = 30$. This refers to exist the region of coalescence

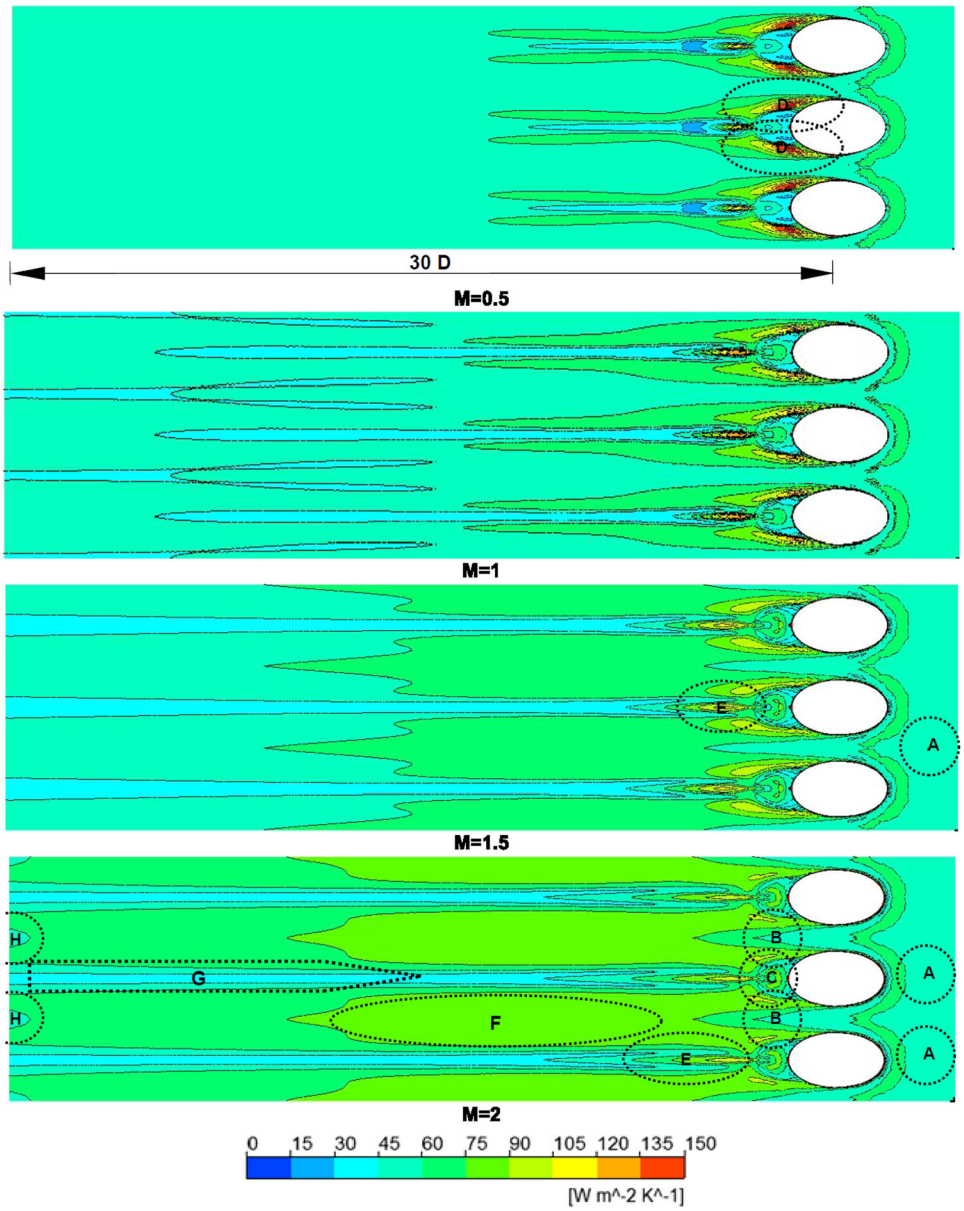

Fig. 26 Detailed heat transfer coefficient distributions for annular film hole at different blowing ratios

the jets and centerline region leading to decreasing the average heat transfer coefficient values at $X/D = 20$, while at $X/D = 30$ and $M = 1$, the centerline region disappeared and therefore the average values are higher.

Figure 25 shows the variation of NHFR for annular film hole and the experimental results [27] of circular film hole with an upstream heating along streamwise direction (X/D). The trends of each annular hole and experimental circular hole are the same at all blowing ratios. It is clear that the values of NHFR decrease with increasing (X/D) at low blowing ratio. With increasing blowing ratios, the values of NHFR increase with increasing (X/D). This refers to the fact that the jet starts to separate and to reattach over the surface at high blowing ratios. It is clear that the values of NHFR for the annular hole are higher than for the circular hole [27] due to increasing film cooling effectiveness levels for the annular film hole.

Figure 26 shows the detailed heat transfer coefficient distributions for annular film hole at different blowing ratios. In this figure, the low and high heat transfer coefficient regions can be described as follows:

- Region (A)
  This is unaffected region upstream of the hole. The heat transfer is related only to mainstream effects.
- Region (B)
  This region is between two adjacent holes. For $M = 0.5$ and 1, this region is not covered by the injected film so that the heat transfer coefficient remains almost the same

as in a region (A). For $M = 1.5$ and 2, the heat transfer coefficient increases due to coalescence of the jets.
The secondary flow remains separate until $X/D = 30$ at $M = 0.5$, while the secondary flow remains separate and merges at $X/D = 23.7$ and continuous until $X/D = 30$ for $M = 1$. For $M = 1.5$, the secondary flow merges at about $X/D = 4.5$. For $M = 2$, the secondary flow merges at about $X/D = 3$ and this refers to the strong interaction of neighboring jets with each other and with the mainstream.

- Region (C)
  This region is immediately downstream of the injection hole. For $M = 0.5$, minimum heat transfer coefficient occurs due to jet effects to create a stagnation region underneath the jet. For $M \geq$, the heat transfer coefficient increases.
- Region (D)
  This region is along the sides of the injection holes. For $M = 0.5$ and 1, higher heat transfer coefficient occurs due to the greater interaction between the mainstream and the secondary flow because the jet still attaches over the surface. For $M > 1$, the jet starts to lift off from the surface leading to region (E).
- Region (E)
  This region is downstream of the injection hole after region C at $X/D = 3$. For $M = 0.5$ and 1, because the jets remain attached near the surface, the wall temperature is low and therefore the heat transfer coefficient is high according to Eq. 19. For $M \geq 1.5$, the wall temperature is high due to increasing mainstream jet interaction where the secondary flow lifts off and hinders the mainstream, and the mainstream penetrates underneath the secondary flow and sweeps toward the wall under the injected flow. Therefore, the heat transfer coefficient is low. But the region area becomes larger with increasing blowing ratios. The region length is $1.8D$, $3.1D$, $4.8D$ and $8D$ at $M = 0.5$, 1, 1.5 and 2, respectively.
- Region (F)
  This region is downstream and midway between the holes. For $M = 0.5$ and 1, the heat transfer is related only to mainstream effects and low heat transfer coefficient occurs. For $M = 1.5$ and 2, high heat transfer coefficient occurs due to spreading and merging of two neighboring jets and the interacting vortex structures midway between the holes.
- Region (G)
  This is centerline region. For $M = 0.5$, this region is not available due to mainstream effects only, which are dominated there. For $M = 1$, low heat transfer coefficient occurs, but this region is very limited. For $M = 1.5$ and 2, low heat transfer coefficient occurs due to increasing boundary layer thickness due to the reattached the flow along the centerline.
- Region (H)
  This region is further downstream at midway between the holes. For $M = 0.5$, 1 and 1.5, this region is not available. For $M = 2$, low heat transfer coefficient occurs due to the partial reattachment of the jet to the surface.

6 Conclusions

In the present paper, the film cooling performance with annular film hole is investigated and compared with other configurations. The film cooling effectiveness of the annular film hole outperforms the rectangular and circular film holes at all blowing ratios, especially at $M = 1$, and the average values are 106 and 328.5 %, respectively. The annular film hole shows higher NHFR values at all blowing ratios than the other hole configurations. The low and high heat transfer coefficient regions were described for annular hole in detail. Pressure coefficient profiles showed that the peak pressure of annular film hole is less than of rectangular hole. Contours of the turbulence kinetic energy showed the regions of turbulence levels for annular and rectangular film holes. Velocity profiles showed that the jet velocity components of annular film hole were less than of rectangular film hole, leading to the jet in case of rectangular film hole that penetrates deeper than the jet in case of annular film hole.

Acknowledgments The authors thank the reviewers for useful comments and their efforts.

References

1. Han, J.C.; Dutta, S.; Ekkad, S.: Gas Turbine Heat Transfer and Cooling Technology. pp. 159–239. Taylor & Francis, New York (2013)
2. Saumweber, C.; Schulz, A.; Wittig, S.: Freestream turbulence effects on film cooling with shaped holes. ASME J. Turbomach. **125**, 65–73 (2003)
3. Goldstein, R.J.; Eckert, E.G.; Burggraf, R.: Effects of hole geometry and density on three dimensional film cooling. Int. J. Heat Mass Transf. **17**, 595–607 (1974)
4. Sen, B.; Schmidt, D.L.; Bogard, D.G.: Film cooling with compound angle holes: heat transfer. ASME J. Turbomach. **118**, 800–806 (1996)
5. Thole, K.; Gritsch, M.; Schulz, A.; Wittig, S.: Flowfield measurements for film cooling holes with expanded exits. ASME J. Turbomach. **120**, 327–336 (1998)
6. Laveau, B.; Abhari, R.S.: Influence of flow structure on shaped hole film cooling performance. ASME paper GT2010-23032 (2010)
7. Gao, Z.; Han, J.C.: Influence of film-hole shape and angle on showerhead film cooling using PSP technique. J. Heat Transf. **131**, 1–11 (2009)
8. Elwekeel, F.N.M.; Abdala, A.M.M.; Huang, D.: Upstream and downstream step curvature effects on film cooling effectiveness and flow structures. Arab. J. Sci. Eng. **40**, 3697–3707 (2015)

9. Abdala, A.M.M.; Elwekeel, F.N.M.; Huang D.: Film cooling effectiveness and flow structures for novel upstream steps. Appl. Therm. Eng. pp. 1–14. http://dx.doi.org/10.1016/j.applthermaleng.2015.05.074 (2015)
10. Abdala, A.M.M.; Elwekeel, F.N.M.: An influence of novel upstream steps on film cooling performance. Int. J. Heat Mass Transf. **93**, 86–96 (2015)
11. Ely, M.J.; Jubran, B.A.: A numerical study on increasing film cooling effectiveness through the use of sister holes. ASME paper GT-2008-50366 (2008)
12. Nasir, H.; Achrya, S.; Ekkad, S.: Improved film cooling from cylindrical angled holes with triangular tabs: effect of tab orientations. Int. J. Heat Fluid Flow **24**, 657–668 (2003)
13. Bunker, R.: Film cooling effectiveness due to discrete holes within a transverse trench. ASME paper GT2002-30178 (2002)
14. Abdala, A.M.M.; Zheng, Q.; Elwekeel, F.N.M.: Aerodynamic analysis and validation by using three turbulence models for narrow trench configuration. Heat Mass Transf. **50**, 603–616 (2013)
15. Abdala, A.M.M.; Zheng, Q.; Elwekeel, F.N.M.; Dong, P.: Computational film cooling effectiveness of dual trench configuration on flat plate at moderate blowing ratios. J. Mar. Sci. Appl. **12**, 208–218 (2013)
16. Harrison, K.L.; Bogard, D.G.: CFD predictions of film cooling adiabatic effectiveness for cylindrical holes embedded in narrow and wide transverse trenches. ASME paper GT2007-28005 (2007)
17. Waye, S.; Bogard, D.: High resolution of film cooling effectiveness measurements of axial holes embedded in a transverse trench with various trench configurations. ASME J. Turbomach. **129**, 294–302 (2007)
18. Zuniga, H.A.; Kapat, J.S.: Studied effect of increasing pitch-to-diameter ratio on the film cooling effectiveness of shaped and cylindrical holes embedded in trenches. ASME paper GT2009-60080 (2009)
19. Goldstein, R.J.; Jin, P.; Olson, R.L.: Film cooling effectiveness and mass/heat transfer coefficient downstream of one row of discrete hole. ASME J. Turbomach. **121**, 225–232 (1999)
20. Ammari, H.D.; Hay, N.; Lampard, D.: The effect of density ratio on the heat transfer coefficient from a film-cooled flat plate. ASME J. Turbomach. **112**, 444–450 (1990)
21. Hay, N.; Lampard, D.; Saluja, C.L.: Effect of cooling films on the heat transfer coefficient on a flat plate with zero mainstream pressure gradient. ASME J. Eng. Gas Turbine Power **107**, 105–110 (1985)
22. Ekkad, S.V.; Zapata, D.; Han, J.C.: Heat transfer coefficient over a flat surface with air and CO_2 film injection through compound angle holes using a transient liquid crystal image method. ASME J. Turbomach. **119**, 580–586 (1997b)
23. Gritsch, M.; Schulz, A.; Witting, S.: Heat transfer coefficient measurements of film cooling holes with expanded slots. ASME paper GT1998-28 (1998a)
24. Rhee, D.H.; Lee Y.S.; Cho, H.H.: Film cooling effectiveness and heat transfer of rectangular-shaped film cooling holes. ASME paper GT2002-30168 (2002)
25. Wilcox, D.C.: Turbulence Modeling for CFD. DCW Industries Inc., La Canada (1998)
26. Bogard, D.G.: Airfoil film cooling. The Gas Turbine Handbook, National Energy Technology Laboratory, Section 4.2.2.1 (2006)
27. Harrison, K.L.; Dorrington, J.R.; Dees, J.E.; Bogard, D.G.; Bunker, R.S.: Turbine airfoil net heat flux reduction with cylindrical holes embedded in a transverse trench. ASME J. Turbomach. **131**, 1–8 (2009)